Position dependent response of Magnetic Nanoparticles using Magnetic Particle Imaging (MPI)

M.Irfan[1, 2*], O. Mercan Dogan[1, 3], N. Dogan[1, 3]
[1]Applied Medical Imaging Lab (AMIL),
[2]Department of Electronics Engineering,
[3]Department of Physics
Gebze Technical University (GTU)
Kocaeli, Turkey
E-mail: mirfan@gtu.edu.tr

A. Bingolbali[1, 4]
[1]Applied Medical Imaging Lab (AMIL),
[4]Department of Bioengineering
Yildiz Technical University (YTU)
Istanbul, Turkey
E-mail: ab1353@gmail.com

***Abstract*—This paper presents the design and implementation of magnetic particle imaging (MPI) for 1D phantom imaging. Selection field setup, transmit and receive coil is designed and simulated in COMSOL Multiphysics®. Comprehensive analysis of the selection field and homogenous transmit field superposition is carried out in COMSOL. 1D phantom is scanned at different positions inside the field of view (FOV). Optimum signals are achieved at static field free point (FFP) and minimum signals are observed at the boundaries (zero velocity of FFP) of the FOV.**

Keywords—magnetic particle imaging; field of view; field free point.

I. INTRODUCTION

Magnetic Particle Imaging (MPI) is a novel imaging technique that only produces signals from tracer and has no background interference [1]. MPI signals have a linear dependence on the concentration of super-paramagnetic iron oxide nanoparticles (SPIONs). MPI exploits the nonlinear behavior (Langevin function) of magnetization of the SPIONs. This technique promises fast scanning and high spatial resolution with the prospect of 3D real-time imaging. The magnetization of SPIONs is 10 million times higher than nuclear para-magnetism of water (proton) [2] in Magnetic Resonance Imaging (MRI). The average scanning time in MPI is 90 minutes, however, MPI promises less than 1 second.

MPI is a tomographic imaging tool and does not provide structural informal of the subject. However, MRI and computed tomography (CT) are anatomical imaging tools. MPI-MRI hybrid system was implemented [3], but complex hardware demand and longer acquisition time of MRI does not comply with modern-day needs. However, the integration of CT with the MPI technique will shorten the scanning time [4].

MPI devices are in the developing phase and preclinical tests are conducted to explore its limits. It mainly consists of the selection field, drive fields, and tracer material. Intrinsically MPI scanner is 3D in nature due to the selection field [5]. MPI scanner for relaxation-based multi-color mapping was designed [6]. Field free point (FFP) and field free line (FFL) are well-known topologies defined by the selection field characteristics. A voxel-based scan is performed of 3D subject volume using FFP. Angiography, early-stage cancer detection, and functional imaging are promised applications of MPI.

Here, we have been designing an MPI scanner for phantom imaging. FFP based selection field is implemented with two pairs of NdFeB permanent magnets. A homogeneous drive field is achieved with a solenoid coil. MPI signals are sensed with gradiometric type received coil.

II. METHODS

Selection field setup (permanent magnets pair), copper shielding, transmit coil, and receive coil are the main parts of the MPI scanner as shown in Fig. 1.

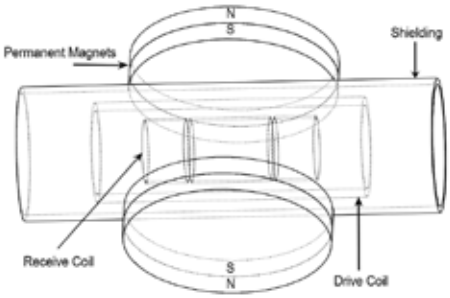

Fig. 1. 3D view of MPI scanner; disk shape permanent magnets (S; south pole, N; north pole) are placed either side of the copper shielding, coaxial drive and receive coils are mounted in the middle (FFP) of the setup.

A. Permanent Magnets Design

Two pairs of NdFeB permanent magnets are used to generate a 4.3 T/m gradient field. The remanent flux density of 0.88 T is chosen for the magnets. Each magnet has a 100 mm diameter and 10 mm thickness. The magnetic strength of the magnets is enhanced by combining two magnets (poles are S-N-S-N of each pair) as shown in Fig. 2.

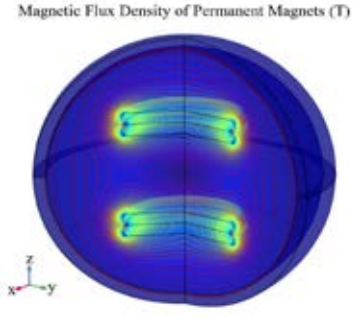

Fig. 2. The magnetic flux density (T) of NdFeB permanent magnets; transparent view from -90° to 225°.

978-1-7281-8073-1/20/$31.00 ©2020 IEEE

The magnets are placed along the z-axis having a 70 mm distance between them according to Maxwell configuration theory. The magnetic fields of both pairs cancel each other at the middle point. The magnetic field strength at the middle point is very weak (minimum) which is also known as FFP as represented in Fig. 3.

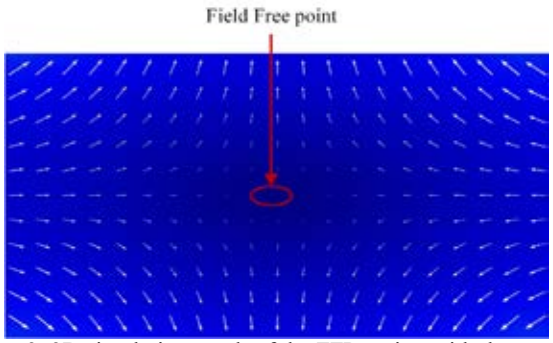

Fig. 3. 3D simulation result of the FFP region with the arrow representation in the y-z plane. The z-axis is represented horizontally while y-axis is represented vertically.

Magnetic field strength is linearly increasing on either side of the FFP along all axes. Gauss's law of electromagnetism describes the divergence of the magnetic field. The asymmetry of the gradient field values produces a cubic shape field of view (FOV) to scan objects. Gradient field strength along the z-axis as displayed in Fig. 4. The gradient of the selection field (4.3 T/m) is 40 mm homogeneous around the FFP (z = 0). Due to the asymmetry of magnetic fields, the gradient field along x and y axes is -2.15 T/m.

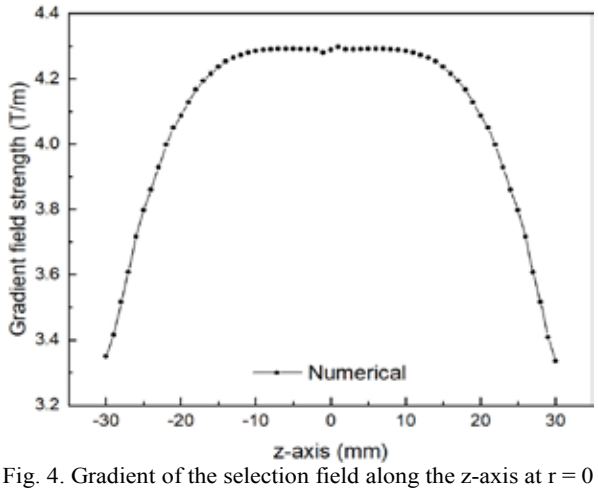

Fig. 4. Gradient of the selection field along the z-axis at r = 0 mm line.

B. Transmit and Receive Coil

The transmit coil is implemented with an electromagnetic solenoid to generate a homogeneous excitation field at an operating frequency of 9.3 kHz. The coil is designed and simulated in COMSOL Multiphysics® to produce a 15 mT magnetic field as demonstrated in Fig. 5.

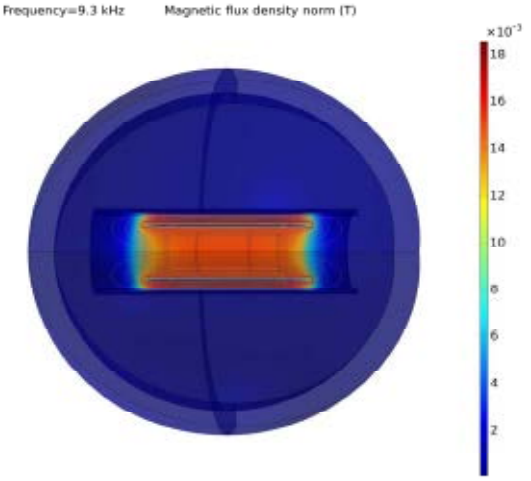

Fig. 5. Magnetic flux density of the drive coil. Inner most structure is 3-section based gradiometric receive coil. Middle structure is drive coil, which is the source of magnetic field, enclosed by the copper shielding.

Litz wire is used for the implementation of both coils to minimize the effect of skin depth. Sensitivities of the coils are calculated in COMSOL with direct current feeding of 1A. To prevent the drive and receive coils from the nonlinearities of the permanent magnets and environment electromagnetic interferences, cylindrical copper shielding of 3 mm thickness is used. Moreover, shielding also restrains high-frequency magnetic fields in a closed area. The effects of shielding are analyzed, and the results are presented in Fig. 6.

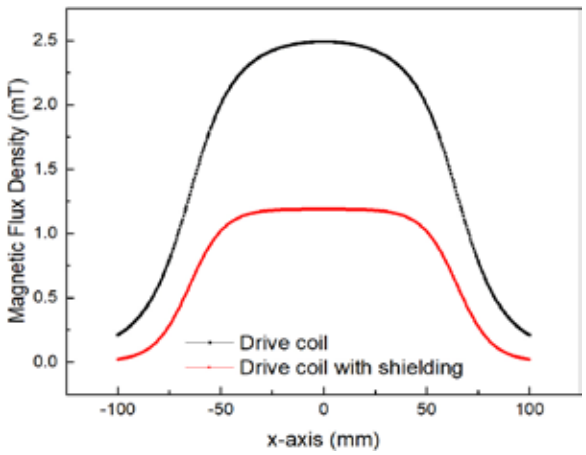

Fig. 6. Sensitivity of the drive coil w/ and w/o copper shielding. 1A direct current was applied to standalone drive coil, while 1A alternating current was applied w/ shielding.

The isolated transmit coil has obtained a sensitivity of 2.49 mT/A. However, shielding reduces the sensitivity of 1.18 mT/A and increases the homogeneity of the magnetic field at high-frequency alternating current. The drawback of reduced sensitivity of the drive coil is eliminated with the implementation of the selection field with electromagnets instead of permanent magnets. So, there will be no need for copper shielding that causes a reduction in sensitivity. Similarly, the sensitivity of a single layer receive coil is also

simulated in COMSOL. The central section of the receive coil is double in length and the wire turns as compared to oppositely wounded outer sections. Hence, a maximum sensitivity of 1.01 mT/A is achieved from the middle section.

III. Field Free Point Movement

The selection field setup produced fixed FFP, however, it is superimposed with a dynamic magnetic field of drive coil which controls the movement of the FFP. Extreme limits of the FFP defined the FOV region. The virtual movement of FFP over half cycle of the drive field is simulated in COMSOL as shown in Fig. 7. It is observed that FFP moves fast in the middle and slowdown at the outer edges. As the drive field is sinusoidal the response on either side of the FFP is symmetric. FOV region along the x-axis varies from -7 mm to 7 mm. Theoretically, a tracer presence near the outer edges does not produce any signal. Maximum signals are induced over the receive coil when magnetic materials are placed in the middle of the FOV (x = 0).

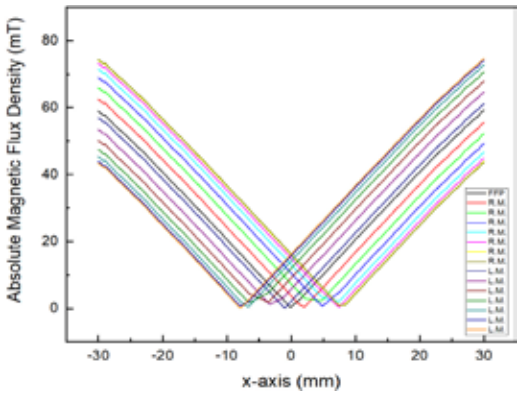

Fig. 8. The field free point (FFP) is moved on the either side depends upon the magnitude of the drive field. R.M. represents right moving while L.M. stands for left moving.

Phantom Imaging

MPI scanner is implemented after the optimization of the hardware components as shown in Fig. 8. Initially, 9.3 kHz operating frequency is selected for phantom imaging of the standard Vivotrax magnetic particles. A phantom of 3.5 mm diameter, and 4 mm height having 40 µl SPIONs was translated with a 3D actuator. A homogeneous excitation field of 15 mT was applied through AE 7224 power amplifier. Low-level signals across the receive coil were amplified and filtered with low noise amplifier SR 560. Recorded signals of the samples were further processed background signals were subtracted, and frequency selection filtered was applied in the digital domain. Received signals after analog and digital filtering are displayed in Fig. 9.

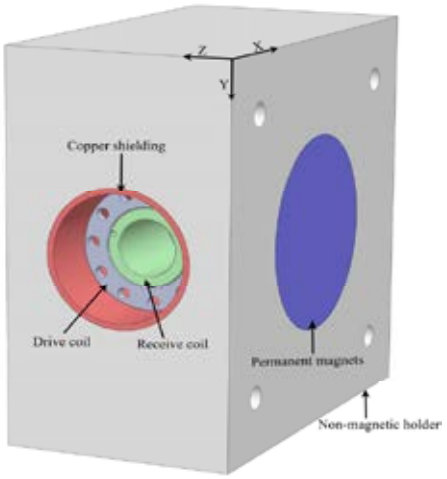

Fig. 9. MPI scanner for 1D phantom imaging. Solenoid drive and gradiometric receive coils are mounted at along bore axis (x-axis). Phantom having magnetic nanoparticles is translated along x-axis with 3D actuator.

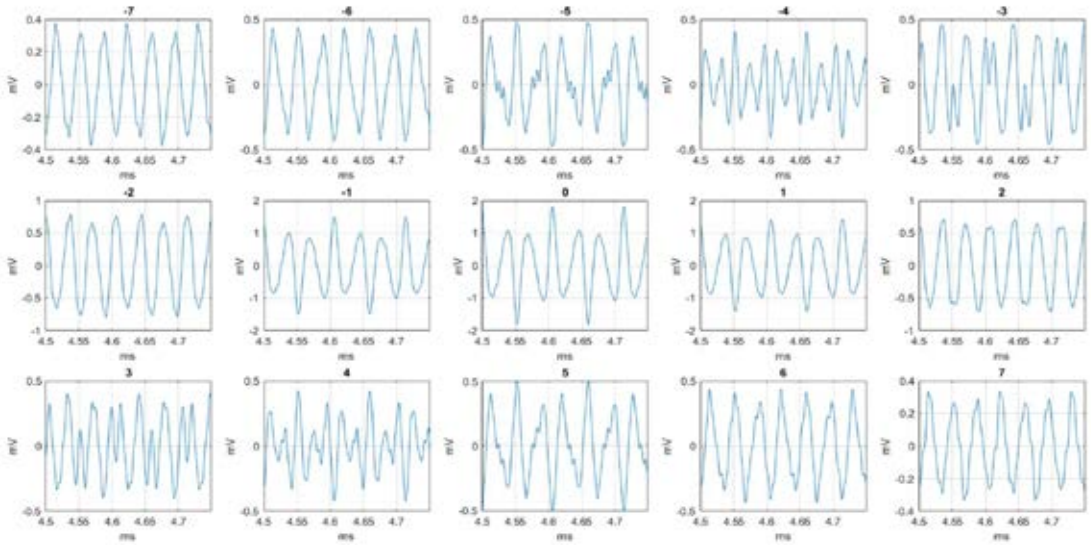

Fig. 7. The response of Vivotrax superparamagnetic iron oxide nanoparticles (SPIONs) inside field of view (FOV). Filtered signals in time domain of receive coils from -7 mm to 7mm along x-axis with 1 mm distance gap between them. Zero index (0) has the highest intensity which is middle of the FOV.

To distinguish recorded signals from various locations were analyzed in the frequency domain. To protect the signals from electronic noise only 20 harmonics were considered and their magnitudes in logarithmic scales are shown in Fig. 10.

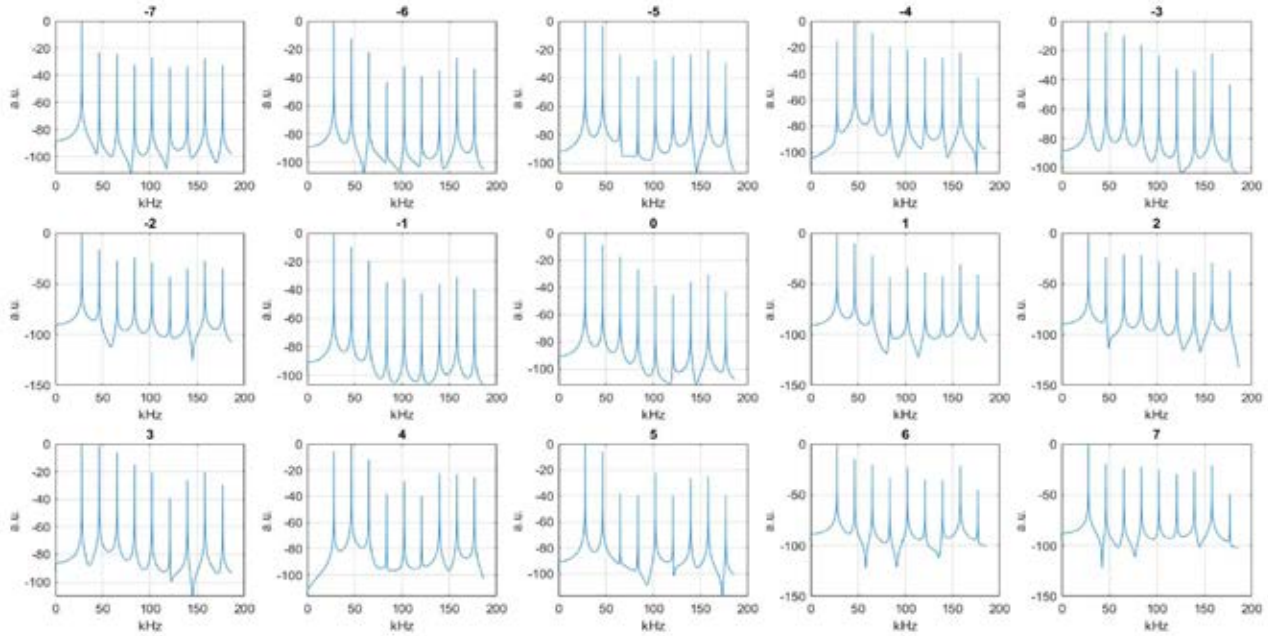

Fig. 10. Odd harmonics response of the magnetic particle imager (MPI) signals. Fundamental harmonics of 9.3 kHz is discarded to eliminate feedthrough.

As the phantom is moved away from the middle-point, the strength and quality of the signal are faded. Received signals appeared at 6, 7, -6 and -7 indexes are seemed to be interference signals. These positions do not have a magnetic nanoparticle response. The velocity of the virtual FFP is not constant, so signals measured from other locations are velocity compensated in the post-processing stage of data analysis. Inside FOV partial overlapping between consecutive sample positions is another phenomenon that complicates post-processing. Thin phantoms, highly sensitive hardware, and SPIONs having sharp magnetization can increase the efficiency of the overall process.

IV. Conclusion

MPI scanner for phantom imaging was designed and implemented. COMSOL Multiphysics® is used as a numerical simulation tool in this research work. Copper shielding effects over excitation field sensitivity and homogeneity were numerically analyzed. Optimized designing parameters were utilized to implement the scanner. 1D phantom of 40 µl Vivotrax was scanned at 15 different positions inside the FOV. Maximum signals were sensed at the center of the FOV. Due to symmetry of the design and sinusoidal excitation field, signals at 1 mm to 7 mm on the right side are equivalent to -1 mm to -7 mm on left side positions.

Acknowledgment

This work was supported by the Scientific and Technological Research Council of Turkey under TUBITAK Grants 115E776 & 115E777.

References

[1] B. Gleich and J. Weizenecker, "Tomographic imaging using the nonlinear response of magnetic particles," Nature, vol. 435, no. 7046, pp. 1214–1217, Jun. 2005.

[2] P. Goodwill, G.C. Scott, P.P. Stang, and S.M. Conolly, "Narrow band magnetic particle imaging," IEEE Transactions of Medical Imaging, vol. 28, NO. 8, August 2009.

[3] J. Franke et al, "System Characterization of a Highly Integrated Preclinical Hybrid MPI-MRI Scanner." IEEE TMI. 35(9), 1993–2004 (2016).

[4] P. vogel et al, "Magnetic Particle Imaging meets Computed Tomography: first simultaneous imaging." Nature, 9:12627 (2019).

[5] J. Weizenecker, B. Gleich, J. Rahmer, H. Dahnke, and J. Borgert, "Three-dimensional real-time in vivo magnetic particle imaging." Phys. Med. Biol. 2009 Feb.54(no. 5):L1–L10.

[6] Y. Muslu, M. Utkur, O. B. Demirel and E. U. Saritas, "Calibration-free relaxation-based multi-color magnetic particle imaging," IEEE Transactions on Medical Imaging, vol. 37, no. 8, August 2018.